Efficient and Effective Ultrasound Image Analysis Scheme for Thyroid Nodule Detection

Eystratios G. Keramidas, Dimitris K. Iakovidis, Dimitris Maroulis, and Stavros Karkanis

Dept. of Informatics and Telecommunications, University of Athens, Panepistimioupolis, 15784, Athens, Greece
rtsimage@di.uoa.gr

Abstract. Ultrasound imaging of thyroid gland provides the ability to acquire valuable information for medical diagnosis. This study presents a novel scheme for the analysis of longitudinal ultrasound images aiming at efficient and effective computer-aided detection of thyroid nodules. The proposed scheme involves two phases: a) application of a novel algorithm for the detection of the boundaries of the thyroid gland and b) detection of thyroid nodules via classification of Local Binary Pattern feature vectors extracted only from the area between the thyroid boundaries. Extensive experiments were performed on a set of B-mode thyroid ultrasound images. The results show that the proposed scheme is a faster and more accurate alternative for thyroid ultrasound image analysis than the conventional, exhaustive feature extraction and classification scheme.

Keywords: Ultrasound, Thyroid Nodules, Thyroid Boundary Detection, Local Binary Patterns.

1 Introduction

Thyroid is a small gland located near the bottom of the neck. It produces hormones that affect heart rate, cholesterol level, body weight, energy level, mental state and a host of other conditions. Epidemiologic studies have showed that palpable thyroid nodules occur in approximately seven percent of the population, but nodules found incidentally on ultrasonography suggest a prevalence up to 67 percent [1]. Ultrasound imaging (US) can be used to detect thyroid nodules that are clinically occult due to their size or their shape. However, the interpretation of US images, as performed by the experts, is still subjective. An image analysis scheme for computer aided detection of thyroid nodules would contribute to the objectification of the US interpretation and the reduction of the misdiagnosis rates.

Early approaches to US image analysis utilized local grey-level histogram information for the characterization of the histological state of the thyroid tissue [2]. Subsequent approaches were based on spatial, first and second order statistical features [3][4] as well as on frequency domain features for computer aided diagnosis of lymphocytic thyroiditis [5]. Recent approaches include quantification of thyroid

M. Kamel and A. Campilho (Eds.): ICIAR 2007, LNCS 4633, pp. 1052–1060, 2007.

tissue characteristics using co-occurrence matrix features [6], and active contour methodologies for fine delineation of thyroid nodules [7]. However, many of them require manual selection of Regions Of Interest (ROI) within the US image, and they usually involve intensive computations, such as exhaustive feature extraction, or iterative integral operations over the whole image.

In this paper we propose a novel scheme for automatic nodule detection based on features extracted from longitudinal US images of thyroid gland. It involves two phases: a) application of a novel algorithm for the detection of the boundaries of the thyroid gland, and b) detection of thyroid nodules via classification of textural feature vectors extracted only from the ROI defined by the thyroid boundaries. The textural characteristics of the thyroid tissue are encoded by histograms of Local Binary Patterns (LBP) [8]. The advantages of this novel scheme include increased accuracy in nodule detection, compared with the conventional ultrasound image analysis methods, and time efficiency.

The rest of this paper is organized in three sections. Section 2 describes the proposed scheme for the detection of nodules in thyroid gland.. The results from the experimental evaluation of the proposed scheme on thyroid US images are apposed in Section 3. Finally, the conclusions as well as future perspectives are summarized in Section 4.

2 Thyroid Ultrasound Image Analysis Scheme

2.1 Thyroid Boundaries Detection Algorithm

The lobes of the thyroid gland are surrounded by a thin fibrous capsule of connective tissue [9]. That capsule bounds the thyroid gland and can be identifiable in longitudinal US images as thin hyperechoic lines. The first phase of the proposed thyroid US image analysis scheme aims to the detection of those hyperechoic lines. Detection is performed by a novel Thyroid Boundaries Detection (TBD) algorithm. This algorithm involves three stages: a) pre-processing of the US image, b) analysis of the pre-processed image, and c) identification of the thyroid boundaries.

In the pre-processing stage, a US input image of $N \times M$ pixels and G grey levels, is normalized and uniformly quantized into z discrete grey levels. Let p_i be the original value of a pixel and q_i the value of that pixel after quantization. Then q_i can be computed as follows:

$$q_i = \frac{G \cdot g}{z-1} : g \in \mathrm{N}, \quad \frac{g \cdot G}{z} \le p_i \le \frac{(g+1) \cdot G}{z} \tag{1}$$

Grey level quantization results in a rough segmentation of the US image and accentuates the hyperechoic bounds of the thyroid gland (Fig. 1b).

In the second stage of the algorithm, the quantized image is vertically sampled from top to bottom with horizontal stripes (Fig 1c). Each stripe has h pixels height and M pixels width, spanning the entire width of the image. A step of $s \in (0, h]$ pixels between two successive stripes is considered, leading to a total of K stripe samples per image.

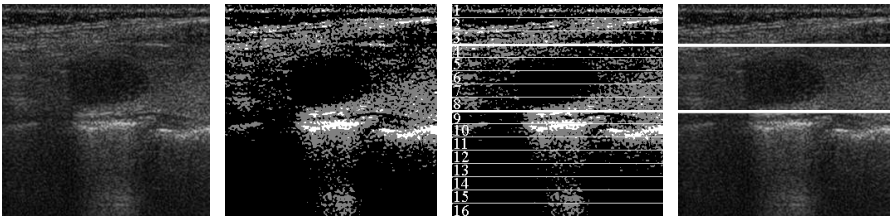

(**a**) (**b**) (**c**) (**d**)

Fig. 1. a) Input thyroid US image digitized at 256 grey levels. (b) Pre-processed US image, quantized at 3 grey levels. (c) Horizontal stripes sampled from the pre-processed image for analysis. (d) The detected thyroid boundaries superimposed to the original input image.

For each stripe, a weighted sum I_n is computed, where n denotes the stripe index incrementing from top ($n = 1$) to bottom ($n = K$) (Fig. 1c). The weighted sum of the number of pixels with grey level j, for each stripe n is calculated by the following equation:

$$I_n = \sum_{j=0}^{G} \left(w(j) \cdot \sum_{P_{j,n}} 1 \right) \tag{2}$$

where $P_{j,n}$ represents the set of pixels having grey level j and reside within stripe n.

In Eq. 3, $w(j)$ denotes a quadratic weight function, which is defined as $w(j) = a \cdot j^2 + \beta \cdot j + \gamma$, where α, β, γ are constants. The choice of the optimal weight function has been considered so as to amplify the contribution of higher grey levels in the calculation of I_n. Constants β, γ are chosen so as to satisfy $(w, j) = (0, 0)$ and $(w, j) = (1, G)$. Therefore $w(j)$ is finally derived by the following equation:

$$w(j) = a \cdot j^2 + \frac{1 - a \cdot G^2}{G} j \tag{3}$$

This weight function aims to amplify the contribution of higher grey levels, which clearly appear as hyperechoic lines in US images after the quantization process of the first stage (Fig 1c).

The values of I_n for the stripes sampled from the US image of Fig. 1, are depicted in Fig. 2. From this figure, it can be noticed that the peak values of I_n correspond to the stripes that fall on the thyroid boundaries.

A direct measure of the rate of change of I_n, between two successive stripes is estimated as follows:

$$D_n = \left. \frac{d(I_i)}{di} \right|_{i=n} \cdot I_n, \; n = 1,2,...K \tag{4}$$

In the final stage of the algorithm, the stripes that contain the outer and the inner thyroid boundaries are selected. If n_{outer} and n_{inner} are the stripe indices that correspond to the outer and the inner boundaries respectively, then n_{outer} and n_{inner} should satisfy the following conditions:

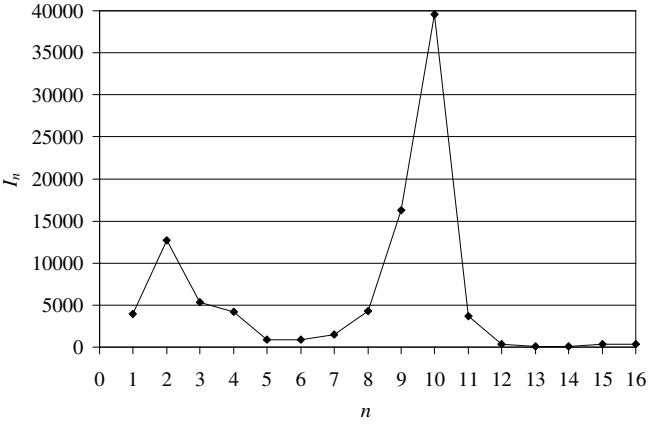

Fig. 2. Example of I_n values for each stripe of the longitudinal US image of figure 1

$$\begin{cases} n_{outer} = \arg\min_n [D_n \cdot \omega_1(n)] \\ n_{inner} = \arg\max_n [D_n \cdot \omega_2(n)] \\ n_{inner} - n_{outer} > T, \quad where\ T > 0 \end{cases}. \tag{5}$$

$$\omega_1(n) = \begin{cases} \log\left(\frac{\lambda \cdot K - n}{\lambda \cdot K} + 1\right) & n < \lambda \cdot K \\ 0 & n \geq \lambda \cdot K \end{cases} \tag{6}$$

$$\omega_2(n) = \begin{cases} \log\left(\frac{n - (1-\lambda) \cdot K}{\lambda \cdot K} + 1\right) & n < (1-\lambda) \cdot K \\ 0 & n \geq (1-\lambda) \cdot K \end{cases} \tag{7}$$

$$\lambda = 1 - \frac{T}{N} \tag{8}$$

Threshold T represents a minimum anteroposterior diameter of the thyroid gland and ensures that stripe n_{inner} will always reside below stripe. n_{outer}. The logarithmic weight functions $\omega_1(n)$ and $\omega_2(n)$ are bias n_{outer} and n_{inner} towards the upper and lower image regions, respectively.

2.2 Detection of Thyroid Nodules

The boundaries detected by the TBD algorithm define a ROI in which feature extraction and classification take place. This ROI is raster scanned with sliding windows (Fig. 3), and from each window a textural feature vector is extracted.

The feature extraction method used for texture analysis of the thyroid gland is based on Local Binary Patterns (LBP). This method was chosen because it produces

highly discriminative texture descriptors, it involves low complexity computations, and it has been successfully applied for ultrasound image analysis [10].

Feature extraction is succeeded by classification of the feature vectors into two classes; a class of normal tissue regions, and a class of nodular tissue regions. A simple *k*-nearest neighbor (*k*-NN) algorithm was chosen as a powerful and robust non-parametric classification method with well-established theoretical properties that has demonstrated experimental success in many pattern recognition tasks [11]. As the LBP feature vectors are actually statistical distributions, the *k*-NN algorithm uses the intersection of two distributions as an effective similarity measure [12]. This measure is estimated by the following equation:

$$\mu(h_1, h_2) = \sum_{n=1}^{L} \min\left(h_1(n), h_2(n)\right) \tag{10}$$

where h_1 and h_2 are the two LBP distributions compared, and L is the number of bins of each distribution.

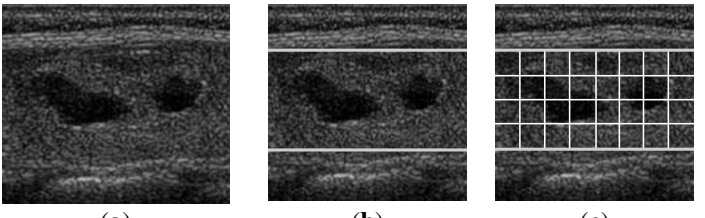

(**a**) (**b**) (**c**)

Fig. 3. (a) Longitudinal US image of thyroid gland. (b) ROI defined by the TBD algorithm. (c) Raster scanned ROI with sliding windows for feature extraction.

3 Results

Thyroid US examinations were performed using a digital US imaging system HDI 3000 ATL with a 5-12 MHz linear transducer at the Department of Radiology of Euromedica, Greece. A total of 39 longitudinal in vivo digital thyroid US images were acquired at a resolution of 256×256 pixels with 256 grey-level depth. The dataset used in the experiments is comprised of various thyroid nodules classified as Grade 3 [13].

In order to obtain ground truth images for the experiments, three expert radiologists manually annotated the US images by drawing horizontal lines for the inner and the outer boundaries of the thyroid lobe, and by delineating the existing thyroid nodules. The ground truth images were generated according to the principle that every pixel is characterized either as normal thyroid parenchyma, thyroid nodule or tissue not belonging to thyroid gland, only if at least two out of three expert radiologists characterized it that way [14]. As a measure of detection accuracy, we consider the overlap between the detected and the ground truth region.

The results of the proposed thyroid US image analysis scheme are presented in two parts, according to the experiments performed. The first part presents the results of the

experimental evaluation of the TBD algorithm, whereas the second part presents the results of the proposed scheme for thyroid nodule detection.

3.1 Evaluation of the TBD Algorithm

Experiments were performed to determine the optimal stripe dimensions that minimize the error between the boundaries detected by the TBD algorithm and the ground truth boundaries. In all the experiments a total of $z = 3$ quantization levels was found to be sufficient. Figure 4 illustrates the results obtained for different combinations of $h \in H$ and $s \in H$: $s \leq h$, where $H = \{4, 8, 16, 32, 64\}$.

The optimal values of the investigated parameters were found to be $h = 16$ and $s = 16$ pixels, for which the mean accuracy in the detection of thyroid boundaries reaches a maximum of 93.2±3.2%. For large values of h (>32) a notable decrement of the accuracy is observed as the large stripe size leads to a gross localization of the thyroid boundaries.

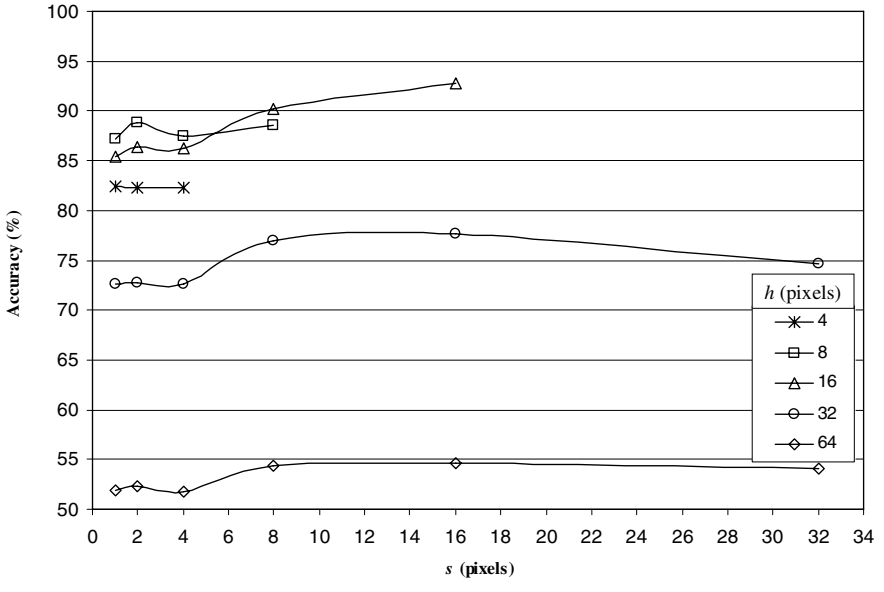

Fig. 4. Mean accuracy of the TBD algorithm for different values of h and s

3.2 Evaluation of the Proposed Scheme for Thyroid Nodule Detection

Experiments were performed to evaluate the performance of the proposed scheme with the TBD algorithm in comparison with the conventional, exhaustive feature extraction scheme. The window sizes tested were 16×16, 32×32 and 64×64 pixels, for sliding steps of 4, 8, 16, 32, 64 pixels. Three LBP neighborhoods, namely 3×3, 5×5, and 7×7 pixels, and three k-NN classifiers for $k = 3, 5, 7$ were tested. The parameters

delivering the best results in Section 3.1 were used for the TBD algorithm i.e. $s = 16$ and $h = 16$.

A balanced proportion of normal and abnormal samples was extracted from the available US images in a way that all samples corresponding to nodular thyroid tissues were included and an equal number of samples corresponding to normal tissues was randomly selected. In [15], it has been shown that learning from a balanced class distribution the classifiers generally come up with fewer but more accurate classification rules for the minority class than for the majority class. So, as the nodular tissue samples comprise a minority class, such an approach is expected to enhance the classification of abnormal samples and thus increase the system's sensitivity.

The best results obtained per LBP neighborhood are summarized in Table 1. It can be observed that in all cases the application of the TBD algorithm improves nodule detection accuracy. The smallest LBP operator, for windows of 32×32 pixels sliding with a step of 8 pixels, resulted in the highest accuracy.

Table 1. Best classification results

Method	Window/ Step	K (*k*NN)	Without TBD Algorithm			With TBD Algorithm		
			Acc/cy	Sens/ty	Spec/ty	Acc/cy	Sens/ty	Spec/ty
$LBP_{\{3\}}$	32/8	7	0.75	0.75	0.76	0.82	0.78	0.81
$LBP_{\{5\}}$	32/4	7	0.74	0.63	0.83	0.81	0.74	0.87
$LBP_{\{7\}}$	32/8	5	0.71	0.62	0.77	0.81	0.73	0.88

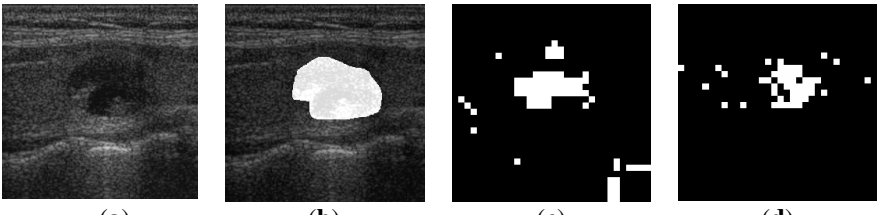

(**a**) (**b**) (**c**) (**d**)

Fig. 5. (a) Longitudinal US image of thyroid gland with a nodule. (b) Ground truth thyroid nodule annotated by radiologists. (c) Classification result without TBD (d) Classification result with TBD. The nodular tissues detected are colored white.

An example detection of a single nodule with and without the TBD algorithm is illustrated in Fig. 5.

Besides the notable improvement of the detection accuracy, the use of the TDB algorithm led also to a notable improvement in time performance, which reached 74%.

4 Conclusions

We presented a novel scheme for nodule detection on longitudinal US images of the thyroid gland. This method encompasses two consecutive phases: utilizing TBD algorithm to detect thyroid boundaries defining an initial ROI and then applying feature extraction and classification techniques within the region defined. Through a series of experiment presented, the proposed scheme proved to be more accurate and less time consuming in nodule detection, compared with the conventional US image analysis methods.

The results of the experimental study presented in this paper lead to the following conclusions about the proposed scheme:

- The proposed scheme can improve nodule detection accuracy.
- The proposed scheme can considerably decrease processing time needed for nodule detection.
- Its application clinical practice is feasible and could contribute to the reduction of false medical decisions.

Future work and perspectives include:

- Experimentation to determine the optimal feature extraction and classification methods for thyroid nodule detection.
- The performance of the proposed scheme will be investigated on images acquired from different US imaging systems.
- Enhancement of the functionality of the proposed TBD algorithm, to deal with other US images beside the longitudinal US images of thyroid gland.
- Evolvement of the proposed time efficient scheme for application in an integrated real time system for the assessment of the thyroid gland.

Acknowledgments. We would like to thank Dr. N. Dimitropoulos, M.D. and EUROMEDICA S.A., Greece for the provision of part of the medical images. This work was supported by the Greek General Secretariat of Research and Technology and the European Social Fund, through the PENED 2003 program (grant no. 03-ED-662). It is also partially supported by the European Social Fund and National Resources – (EPEAEK II).

References

1. Welker, M.J., Orlov, D.: Thyroid Nodules. American Family Physician 67(3) (2003)
2. Mailloux, G.E., Bertrand, M., Stampfler, R.: Local Histogram Information Content Of Ultrasound B-Mode Echographic Texture. Ultrasound in Medicine and Biology 11(5), 743–750 (1985)
3. Wagner, R.F., Insana, M.F., Brown, D.G.: Unified approach to the detection and classification of speckle texture in diagnostic ultrasound. Opt. Eng. 25, 738–742 (1986)

4. Fellingham, L.L., Sommer, F.G.: Ultrasonic characterization of tissue structure in the in vivo human liver and spleen. IEEE Transactions Sonics and Ultrasonics 31(4), 418–428 (1984)
5. Smutek, D., Sara, R., Sucharda, P., Tjahjadi, T., Svec, M.: Image texture analysis of sonograms in chronic inflammations of thyroid gland. Ultrasound in Medicine and Biology 29(11), 1531–1543 (2003)
6. Skouroliakou, C., Lyra, M., Antoniou, A., Vlahos, L.: Quantitative image analysis in sonograms of the thyroid gland. Nuclear Instruments and Methods in Physics Research A 569, 606–609 (2006)
7. Iakovidis, D.K., Savelonas, M.A., Karkanis, S.A., Maroulis, D.E.: Segmentation of Medical Images with Regional Inhomogeneities. In: Proc. International Conference on Pattern Recognition (ICPR), vol. 2, pp. 279–282. IAPR, Hong Kong (2006)
8. Ojala, T., Pietikainen, M., Harwood, D.: A comparative study of texture measures with classification based on feature distributions. Pattern Recognition 29, 51–59 (1996)
9. Rumack, C.M., Wilson, S.R., Charboneau, J.W., Johnson, J.A.: Diagnostic Ultrasound. Mosby (2004), ISBN 0323020232
10. Pujol, O., Radeva, P.: Supervised texture classification for intravascular tissue characterization. In: Suri, J.S., Wilson, D., Laximinarayan, S. (eds.) Handbook of Biomedical Image Analysis. Segmentation Models Part B, vol. 2, Springer, Heidelberg (2005)
11. Theodoridis, S., Koutroumbas, K.: Pattern Recognition. Academic Press, London (1999)
12. Swain, M.J., Ballard, D.H.: Color indexing. IJCV 7(I), 11–32 (1991)
13. Tomimori, E.K., Camargo, R.Y.A., Bisi, H., Medeiros-Neto, G.: Combined ultrasonografhic and cytological studies in the diagnosis of thyroid nodules. Biochimie 81, 447–452 (1999)
14. Kaus, M.R., Warfield, S.K., Jolesz, F.A., Kikinis, R.: Segmentation of Meningiomas and Low Grade Gliomas in MRI. In: Taylor, C., Colchester, A. (eds.) Medical Image Computing and Computer-Assisted Intervention – MICCAI'99. LNCS, vol. 1679, pp. 1–10. Springer, Heidelberg (1999)
15. Weiss, G.M., Provost, F.: The effect of class distribution on classifier learning. Technical Report ML-TR-43. Dept. of Computer Science, Rudgers University (2001)